Photonuclear Data Evaluation of ^{239}Pu

I. Raškinytė, E. Dupont and D. Ridikas
DSM/DAPNIA/SPhN, CEA-Saclay, F-91191 Gif-sur-Yvette Cedex, France

1 Introduction

Both the development and maintenance of nuclear technologies rely on the availability of nuclear data, for example such as energy-dependent reaction cross sections, energy and angular distributions of reaction products, etc. Nuclear data of photo-induced reactions are important for a variety of present or emerging applications. Among them are radiation transport simulation and radiation shielding design of innovative reactors, diagnostics and shielding of plasma in fusion reactors, activation analysis, safeguards and inspection technologies, nuclear waste transmutation. Most of these applications need evaluated cross sections and emission spectra. In terms of incident energies, the giant dipole resonance region below 30 MeV is essential for most applications. In addition, some medical applications request photonuclear data up to 50 MeV. Finally, it is also desirable to have evaluated data extended to 130 MeV for the computer simulation of intense photoneutron sources and to complement the neutron and proton high-energy libraries.

Actinide cross sections evaluations were reviewed in the framework of a specific IAEA coordinated research project (CRP) [1]. Recently, major actinide cross sections and spectra were evaluated in the framework of a collaboration between LANL and CEA [2] using the Gnash code [3, 4]. These evaluations were done for incident photon energies up to 20 MeV.

New evaluations on ^{235}U and ^{232}Th beyond 20 MeV are described in previous reports [5, 6]. This document presents cross sections calculations up to 130 MeV for ^{239}Pu using the Talys code [7].

2 Reaction mechanisms

In a photoreaction, the ^{239}Pu nucleus is excited by the absorption of a photon. When the excitation energy is large enough, the nucleus can emit neutrons, charged particles, gamma rays or undergo fission. However, the probability to emit charged particles is small due to the high Coulomb barrier of heavy nuclei. The decay chain continues untill all excess energy is released. A schematic representation of the different reaction steps is given in Figure 1.

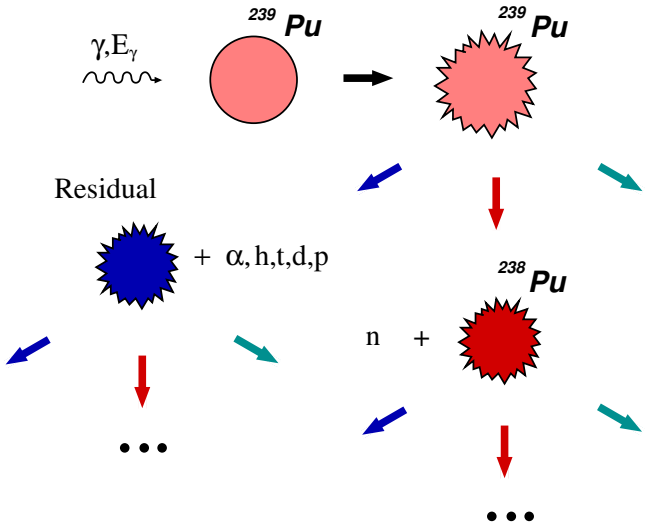

Figure 1: γ+^{239}Pu decay chain. The green (right) arrow corresponds to the fission channel, while red (down) and blue (left) arrows indicate neutron or charged particle emission respectively.

In this work, the photoabsorption process is described by the giant dipole resonance and quasideuteron mechanisms. Preequilibrium particle emission is treated with the classical exciton model. At equilibrium, the compound nucleus decay channels are handled within the Hauser-Feshbach statistical model. Neutron transmission coefficients are calculated with a coupled-channel optical model and fission transmission coefficients are calculated with a double humped parabolic model. The ^{239}Pu cross sections are calculated using the Talys-0.64 code [7], which includes all above mentioned nuclear reaction models.

2.1 Photoabsorption

When modeling photon induced nuclear reactions, the first step is the determination of the photoabsorption cross section. At low energies, below about 30 MeV, the giant dipole resonance (GDR) is the dominant excitation mechanism. At higher energies, up to 140 MeV, the phenomenological model of photoabsorption on a neutron-proton pair (quasideuteron, QD) becomes dominant. Following Chadwick *et al.* [8], the photoabsorption cross section is given by

$$\sigma_{abs}(E_\gamma) = \sigma_{GDR}(E_\gamma) + \sigma_{QD}(E_\gamma). \tag{1}$$

The GDR component of deformed nuclei is given as a sum of two Lorentzians

$$\sigma_{GDR}(E_\gamma) = \sum_{i=1,2} \sigma_{E1,i} \frac{E_\gamma^2 \Gamma_{E1,i}^2}{(E_\gamma^2 - E_{E1,i}^2)^2 + E_\gamma^2 \Gamma_{E1,i}^2}, \tag{2}$$

where $\sigma_{E1,i}$, $E_{E1,i}$, $\Gamma_{E1,i}$ are the GDR peaks' cross section, energy and width respectively.

The QD component is described by the model of Chadwick *et al.* [8] and references therein. In the quasideuteron model it is assumed that photoabsorption takes place on correlated neutron-proton pairs within a nucleus due to the small photon wavelengths and the electric-dipole nature of the interaction. The photoabsorption cross section is expressed in terms of the free deuteron photodisintegration cross section $\sigma_d(E_\gamma)$

$$\sigma_{QD}(E_\gamma) = \frac{L}{A} NZ \sigma_d(E_\gamma) f(E_\gamma), \tag{3}$$

where L is the Levinger parameter and $f(E_\gamma)$ is the Pauli blocking function. NZ is the total number of neutron-proton pairs inside the nucleus, which is multiplied by a reduction factor L/A to take into account that only correlated neutron-proton pairs should be considered. The function $f(E_\gamma)$ accounts for those excitations of neutron-proton pairs that can not occur since the Pauli exclusion principle allows only final particle states above the Fermi level. For derivations of the Pauli blocking function see reference [8].

The photoabsorption cross section in the giant dipole resonance region is fitted to experimental data using expression (2). At higher energies, in the absence of data, the formula (3) with Talys default parameters is used. The GDR parameters can be directly obtained from the experimental photoabsorption cross section or from the sum of partial cross sections. In the latter case light charged particle emission cross sections is assumed to be negligible for heavy nuclei.

All data used in the present evaluation are taken from the EXFOR [9] library. The list of measured cross sections, energy range and references are given in the following table.

Cross section	Energy range [MeV]	Reference
(γ,n)	6.00 – 17.8	B.L. Berman *et al.* [10]
	6.73 – 9.72	M.A.P.V. De Moraes *et al.* [11]
(γ,2n)	12.9 – 17.8	B.L. Berman *et al.* [10]
(γ,f)	5.43 – 9.72	M.A.P.V. De Moraes *et al.* [11]
	6.00 – 17.8	B.L. Berman *et al.* [10]
	7.50 – 11.0	A. Shapiro *et al.* [12]
	4.30 – 6.95	Yu.B. Ostapenko *et al.* [13]
(γ,abs)	6.73 – 9.72	M.A.P.V. De Moraes *et al.* [11]
	7.80 – 19.2	G.M. Gurevich *et al.* [14]

De Moraes and Gurevich [11, 14] directly measured the photoabsorption cross section, whereas Berman *et al.* [10] measured the main partial cross sections: (γ, n), $(\gamma, 2n)$ and (γ, f). Their sum gives the total photoabsorption cross section. For consistency reasons, the Berman results were used to deduce the present GDR parameters. One fit was done with all experimental points (Fit #1, solid line in Fig. 2) and another one without a few points for which the (γ, n) cross section is negative (Fit #2, dashed line in Fig. 2). The solid line falls off more rapidly than the dashed line at energies above 14 MeV. It is related to the energy points for which ^{238}Pu production cross section is negative. In this work the GDR parameters from Fit #2 are used as input to the calculations.

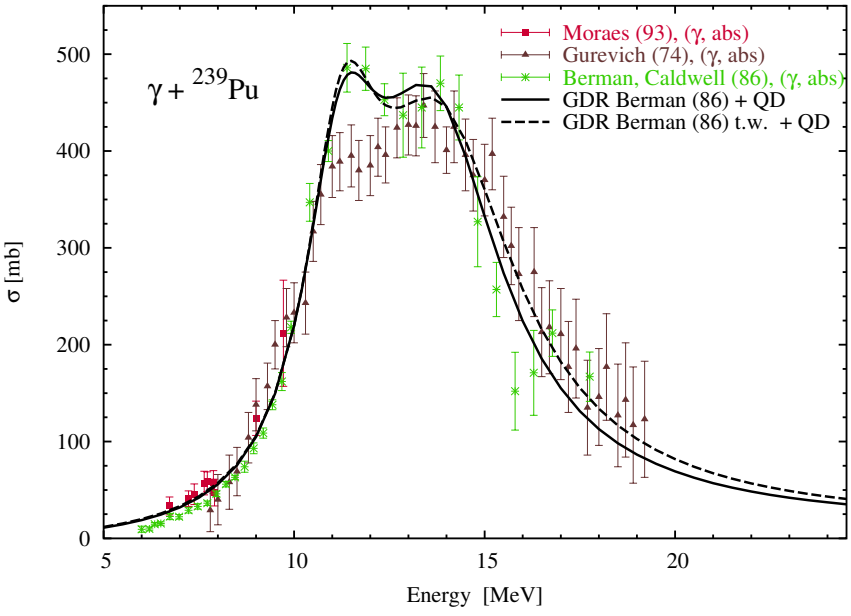

Figure 2: Adjustment of the GDR parameters on the experimental ^{239}Pu photoabsorption cross section (see text).

The GDR parameters obtained in this work are compared with RIPL-2 [15] values in the table below.

E_1 [MeV]	σ_1 [mb]	Γ_1 [MeV]	E_2 [MeV]	σ_2 [mb]	Γ_2 [MeV]	Reference
11.31	373.02	2.55	13.82	368.57	3.69	This work (Fit #1)
11.29	332.97	2.35	13.91	381.74	4.76	This work (Fit #2)
11.28	325.00	2.48	13.73	384.00	4.25	RIPL-2 [15]

2.2 Optical model

Transmission coefficients for the inverse channels are calculated with a global coupled-channels optical potential by Soukhovitskii *et al.* [16]. This potential was developed for neutron-actinide interaction from 1 keV to 200 MeV. Coupling between levels in coupled-channel calculations is due to the deformed nuclear optical potential, where deformation is taken into account through the deformed nuclear shapes

$$R(\theta',\varphi') = R_0 \left\{ 1 + \sum_{\lambda=2,4,6} \beta_{\lambda 0} Y_{\lambda 0}(\theta',\varphi') \right\}, \tag{4}$$

where $Y_{\lambda 0}$ are spherical harmonics and $(\theta',\, \varphi')$ are angular coordinates in the body-fixed frame. The optical potential is of a standard Wood-Saxon shape with real and imaginary volume, imaginary surface and real and imaginary spin-orbit terms [16], namely

$$\begin{aligned}
-V_R f_R(r, R(\theta',\varphi')) &\qquad \text{real volume (R)} \\
-iW_V f_V(r, R(\theta',\varphi')) &\qquad \text{imaginary volume (V)} \\
i4W_D a_D \frac{d}{dr} f_D(r, R(\theta',\varphi')) &\qquad \text{imaginary surface (D)} \\
\left(\frac{\hbar}{m_\pi c}\right)^2 V_{so} \frac{1}{r}\frac{d}{dr} f_{so}(r, R(\theta',\varphi'))\hat{\sigma}\cdot\hat{L} &\qquad \text{real spin-orbit (so)} \\
i\left(\frac{\hbar}{m_\pi c}\right)^2 W_{so} \frac{1}{r}\frac{d}{dr} f_{so}(r, R(\theta',\varphi'))\hat{\sigma}\cdot\hat{L} &\qquad \text{imaginary spin-orbit (so),}
\end{aligned} \tag{5}$$

with the form factors given as

$$f_i(r) = \left[1 + exp((r - R_i(\theta',\varphi'))/a_i)\right]^{-1}, \qquad i = R, V, D, so. \tag{6}$$

Deformed radii R_i are given by equation (4) with $R_0 = r_i A^{1/3}$. However, the spin orbit term is not deformed in standard Talys calculations and in that particular case $R(\theta',\varphi') = R_0$. Well depths V_i as well as r_R are energy dependent. Their functional dependence as well as values of r_i and a_i are

described in the reference [16]. In the latter work, the optical potential parameters were searched for to reproduce available neutron- and proton-induced cross section for ^{238}U and ^{232}Th. Coupled-channels calculations were performed by coupling the first five states of the ground state rotational band. All previous parameters except deformation parameters (adjustable) were used to predict cross sections of other actinides like ^{233}U, ^{235}U, ^{239}Pu, ^{240}Pu and ^{242}Pu.

For the inverse ^{238}Pu+neutron channel we used the deformation parameters given in the reference [16] for the ^{239}Pu nucleus: $\beta_{20} = 0.212$, $\beta_{40} = 0.066$ and $\beta_{60} = -0.0084$. The calculated total neutron cross sections for ^{239}Pu and ^{238}Pu nuclei are shown in Figure 3, where they are compared with experimental ^{239}Pu data. All experimental data are taken from the EXFOR library, where there are records for ^{239}Pu from 0.01 to 30 MeV and no information for ^{238}Pu. This optical potential reproduces well the available measurements from 0.1 MeV to 30 MeV. Below 0.1 MeV, the calculations slightly underestimate the experimental values.

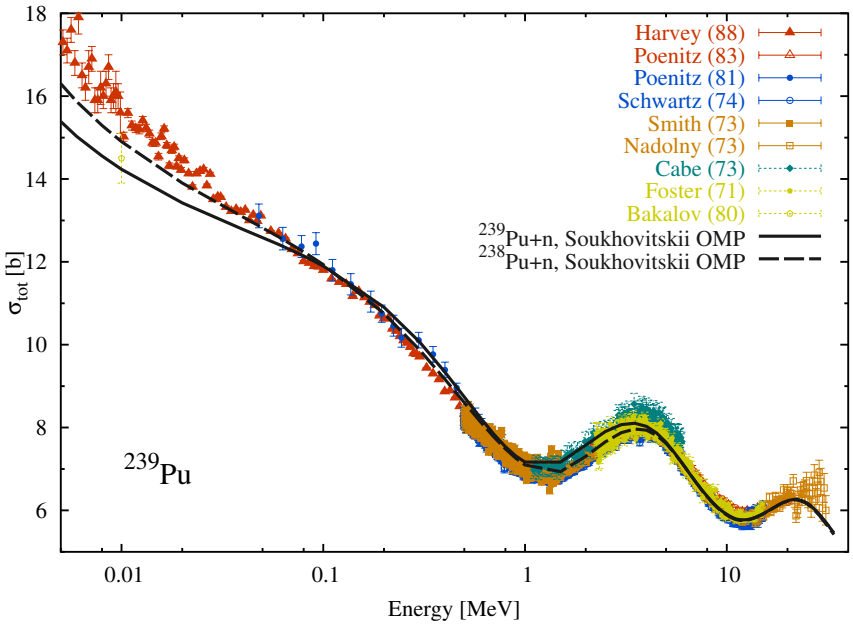

Figure 3: ^{238,239}Pu total neutron cross sections (experimental data are for ^{239}Pu).

Figure 4 shows experimental angular distributions of scattered neutrons on the first three doublets of ^{239}Pu ground-state rotational band. The characteristics of these discrete levels are given in the following table.

Level number	Spin–Parity J^π	Energy [keV]
gs	$1/2^+$	0.0
1	$3/2^+$	7.861
2	$5/2^+$	52.276
3	$7/2^+$	75.706
4	$9/2^+$	163.76
5	$11/2^+$	192.81

Figure 5 gives angular distributions for neutron scattering on ^{239}Pu leading to the excitation of one of the first five levels (see the above table) for 4.0, 4.5, 5.0, 5.5, and 14.1 MeV incident neutron energy. As one can see from these two plots, differential scattering cross sections calculated with Soukhovitskii OMP are also in good agreement with measurements.

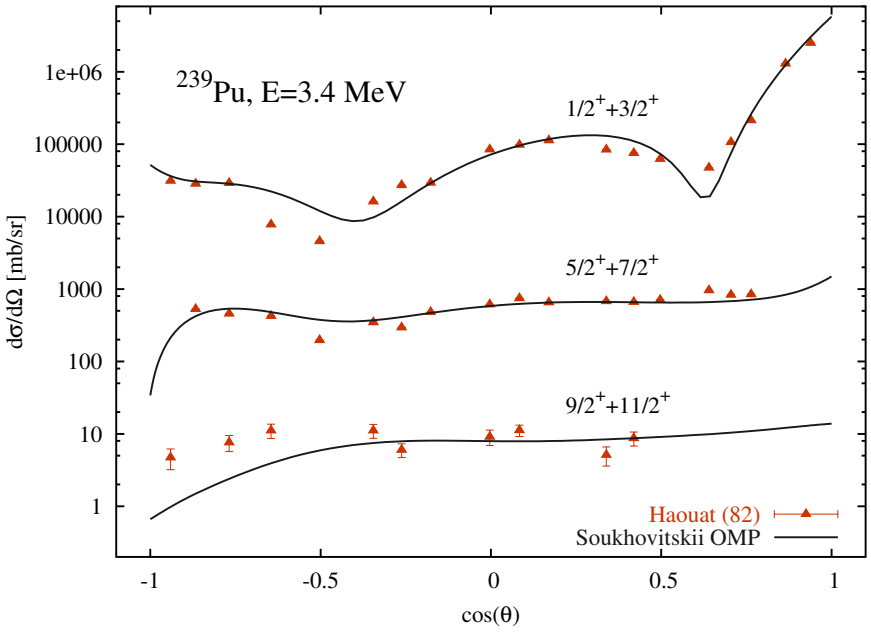

Figure 4: ^{239}Pu differential scattering cross sections on the first three doublets of the ground-state rotational band: $1/2^+(gs) + 3/2^+$, $5/2^+ + 7/2^+$, and $9/2^+ + 11/2^+$ ($E_n = 3.4\ MeV$). The bottom curve and data represent true values, while others are offset by factors 20 (middle curve and data) and 1000 (top curve and data).

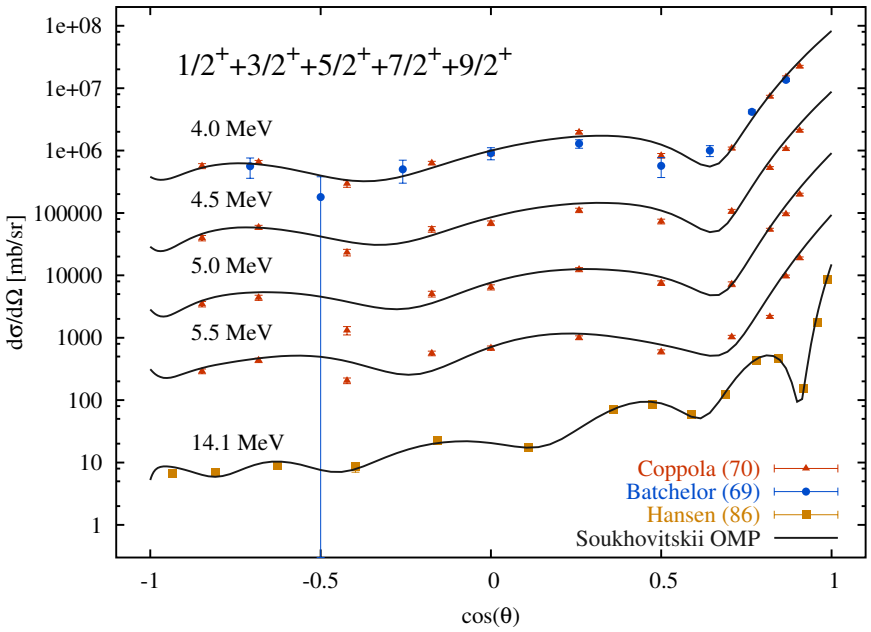

Figure 5: Sum of the ^{239}Pu differential scattering cross sections on the first levels (including gs). The bottom curve and data represent true values, while the others are multiplied by factors 10, 100, etc.

The experimental data against which the optical model potential was checked is given in the table below.

Cross section	Energy [MeV]	Reference
σ_{tot}	$2.78 \cdot 10^{-5} - 0.755$	Harvey *et al.* [17]
	$1.82 - 20.9$	Poenitz *et al.* [18]
	$4.80 \cdot 10^{-2} - 4.81$	Poenitz *et al.* [19]
	$4.65 \cdot 10^{-6} - 2.15 \cdot 10^{-2}$	Bakalov *et al.* [20]
	$0.496 - 15.2$	Schwartz *et al.* [21]
	$0.651 - 1.50$	Smith *et al.* [22]
	$0.5 - 31.0$	Nadolny *et al.* [23]
	$1.11 - 5.99$	Cabe *et al.* [24]
	$2.26 - 15.0$	Foster *et al.* [25]
$d\sigma_{scat}/d\Omega$	14.1	Hansen *et al.* [26]
	3.4	Haouat *et al.* [27]
	4.0, 4.5, 5.0, 5.5	Coppola *et al.* [28]
	4.0	Batchelor *et al.* [29]

2.3 Level densities

Level densities are important ingredients of statistical reaction models. The Talys code includes several level density models. Among these models are: Gilbert-Cameron [30], Fermi gas with deformation-dependent collective effects, HF-BCS [15, 31]. In this work, calculations were done with the Gilbert-Cameron composite formula with energy dependent level density parameter.

In the Gilbert and Cameron level density formulation, the excitation energy range is divided in a low energy part from zero to a matching energy E_M and a high energy part above E_M

$$\rho(E_{ex}) = \begin{cases} \rho_T(E_{ex}), & E_{ex} \leq E_M \\ \rho_F(E_{ex}), & E_{ex} > E_M. \end{cases} \tag{7}$$

At low excitation energy, the model is based on the experimental evidence that the cumulative number of the first discrete levels *vs.* energy can be well reproduced by a constant temperature law. Accordingly, the constant temperature part of the total level densities is given by

$$\rho_T(E_{ex}) = \frac{1}{T} \exp \frac{E_{ex} - E_0}{T}. \tag{8}$$

The nuclear temperature T and E_0 are adjustable parameters. For higher energies, the Fermi-gas model is more suitable and the total level density is then given by

$$\rho_F(E_{ex}) = \frac{\sqrt{\pi}}{12} \frac{\exp(2\sqrt{aU})}{\sqrt{2\pi}\sigma a^{1/4} U^{5/4}}, \tag{9}$$

where $U = E_{ex} - \Delta$, σ^2 is the spin cut-off factor, and a is the level density parameter. In our calculations we used Ignatyuk [32] level density parameter formula

$$a = \tilde{a} \left[1 + \delta W \frac{1 - \exp(-\gamma U)}{U} \right]. \tag{10}$$

The pairing energy Δ, the asymptotic level density value $\tilde{a}$, the shell damping parameter γ and the shell correction energy δW are deduced from Talys systematics [7] or given as input.

The expressions for ρ_T and ρ_F are matched by requiring the continuity of the function $\rho(E_{ex})$ and its derivative at energy E_M. Another constraint is given by considering that the constant-temperature law should reproduce the experimental discrete levels from a lower level N_{low} to an upper level N_{top}. These levels should be chosen such that $\rho_T(E_{ex})$ optimally describes the observed discrete states.

The default Talys level densities were checked against observed levels at low excitation energy. Graphical comparisons for ^{237}Pu, ^{238}Pu and ^{239}Pu are given in Figure 6, 7, and 8 respectively. The level density parameter values used in the present calculations and the default Talys values are given in the table below (default values were used for ^{239}Pu).

	Δ	$\tilde{a}$	γ	δW	N_{low}	N_{top}	Reference
^{237}Pu	0.77948	24.0	0.040	1.20	6	10	This work
	0.77948	25.7	0.074	1.87	2	10	Default
^{238}Pu	1.55569	24.8	0.060	1.20	4	20	This work
	1.55569	25.8	0.074	1.96	2	4	Default
^{239}Pu	0.77622	25.8	0.074	1.84	2	25	Default

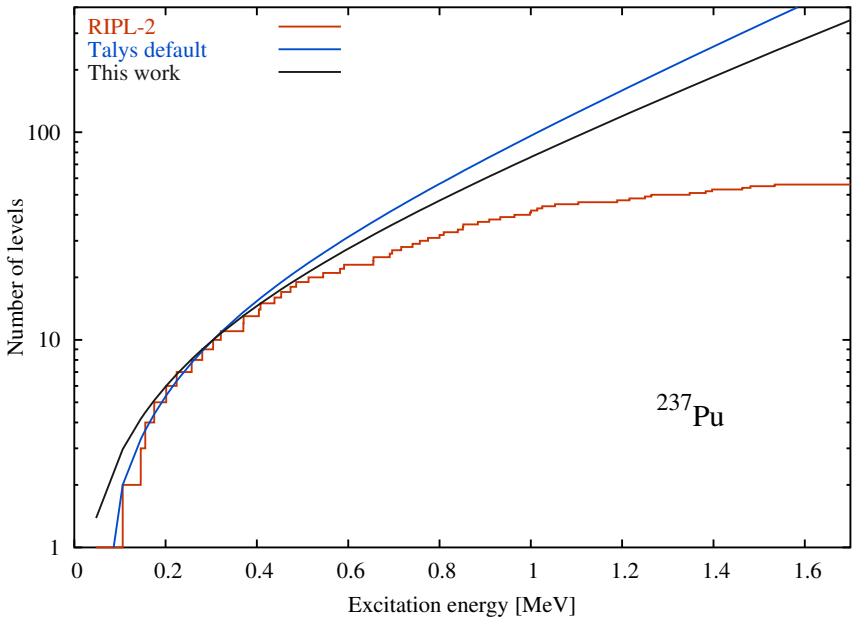

Figure 6: Number of levels *vs.* energy in ^{237}Pu.

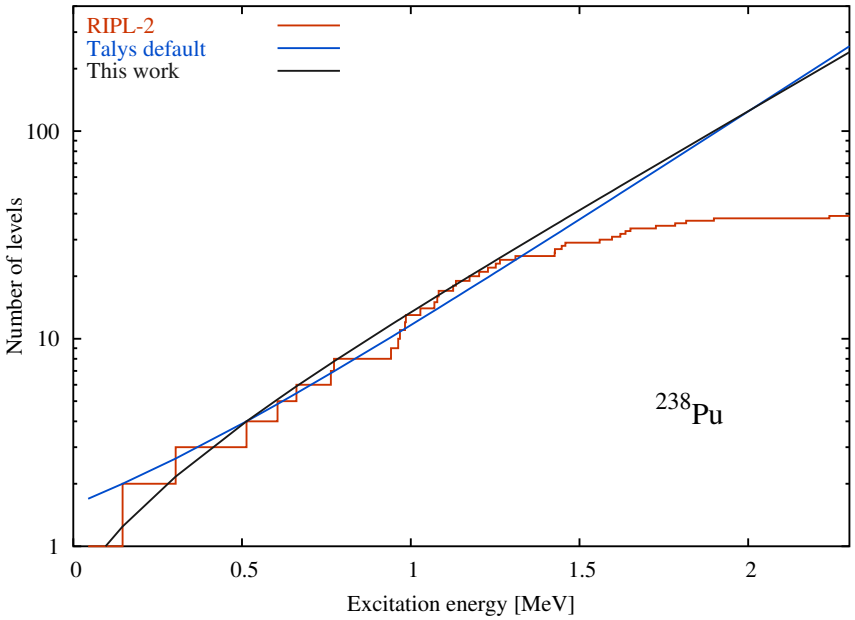

Figure 7: Number of levels *vs.* energy in ^{238}Pu.

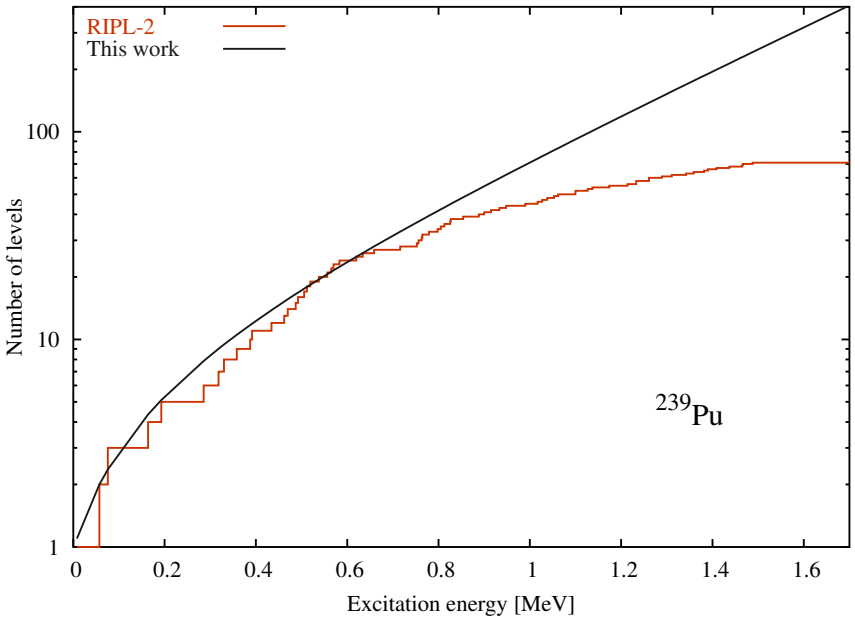

Figure 8: Number of levels *vs.* energy in ^{239}Pu.

2.4 Fission

The fission process is accounted for using a statistical model approach. For present calculations, fission transmission coefficients were calculated with a double humped barrier model. The Hill-Wheeler expression gives the quantum penetrability through a fission barrier described by an inverted parabola

$$T_{HW}(E_{ex}) = \left[1 + exp\left(-2\pi\frac{E_{ex} - B_f}{\hbar\omega}\right)\right]^{-1}, \tag{11}$$

where B_f is the barrier height relative to the nucleus ground state and $\hbar\omega$ is the barrier curvature. For a transition state of energy ϵ_i above the top of the barrier, one simply assumes that the barrier is shifted up by ϵ_i

$$T_{HW}(E_{ex}, \epsilon_i) = \left[1 + exp\left(-2\pi\frac{E_{ex} - B_f - \epsilon_i}{\hbar\omega}\right)\right]^{-1}. \tag{12}$$

For a compound nucleus with excitation energy E_{ex}, spin J, and parity Π, the total fission transmission coefficient is the sum of the individual transmission coefficients for each barrier through which the nucleus may tunnel

$$T_f^{J,\Pi}(E_{ex}) = \sum_i T_{HW}(E_{ex}, \epsilon_i) f(i, J, \Pi) + \int_{E_{th}}^{E_{ex}} \rho(\epsilon, J, \Pi) T_{HW}(E_{ex}, \epsilon) d\epsilon. \tag{13}$$

The summation runs over all discrete transition states on top of the barrier and E_{th} marks the beginning of the continuum. $f(i, J, \Pi) = 1$, if the spin-parity of the transition state equal that of the compound nucleus and 0 otherwise. Moreover, $\rho(\epsilon, J, \Pi)$ are the level densities at an excitation energy ϵ of the fission channels with spin J and parity Π.

In the case of a double humped barrier, one assumes that tunnelling through the barriers A and B can be separated into two independant steps. Then, one calculates the fission transmission coefficients $T_A^{J\Pi}$ and $T_B^{J\Pi}$ using the Hill-Wheeler expression. Finally, the effective fission transmission coefficient is given by the probability to cross the first barrier multiplied by the probability to fission

$$T_{eff}^{J\Pi} = \frac{T_A^{J\Pi} T_B^{J\Pi}}{T_A^{J\Pi} + T_B^{J\Pi}}. \tag{14}$$

In present calculations, the fission barrier heights, widths and transition states were adjusted. The following tables list the barrier heights, widths and transition states used in the present work together with Ripl-2 [15] values.

Barrier heights and widths

Nucleus	This work / RIPL-2 [15]			
	B_{f1} [MeV]	$\hbar\omega_{f1}$ [MeV]	B_{f2} [MeV]	$\hbar\omega_{f2}$ [MeV]
^{239}Pu	6.10 / 6.2	0.8 / 0.7	5.9 / 5.7	0.52 / 0.5
^{238}Pu	6.15 / 5.6	0.3 / 0.9	4.8 / 5.1	0.60 / 0.6
^{237}Pu	5.90 / 5.10	0.8 / 0.7	5.2 / 5.15	0.52 / 0.5

Transition states [This work]

^{238}Pu						^{239}Pu					
First barrier			Second barrier			First barrier			Second barrier		
1	0.00	0^+	1	0.00	0^+	1	0.00	0.5^+	1	0.00	0.5^+
2	0.50	2^+	2	0.50	2^+	2	0.08	2.5^+	2	0.00	0.5^-
3	0.55	0^-	3	0.20	0^-	3	0.05	0.5^-	3	0.08	1.5^+
4	0.55	1^-	4	0.50	1^-	4	0.00	1.5^-	4	0.08	1.5^-
5	0.55	2^-							5	0.00	2.5^+
									6	0.00	2.5^-

3 Results

This paragraph summarizes the results obtained for the ^{239}Pu cross sections evaluation.

The photoabsorption cross section was discussed in section 2.1. We use GDR parameters deduced from Berman *et al.* data [10], excluding energy points for which the (γ, n) cross section is negative.

The optical model for inverse channel calculations was described in section 2.2. In our calculations we use the first five states of the ground state rotational band. The ^{238}Pu deformation parameters are the same as those given in [16] for ^{239}Pu. The ^{238}Pu+neutron transmission coefficients were also used for the ^{237}Pu+neutron exit channel. This approximation does not affect significantly the calculated cross sections. Calculations were done with default Talys spherical OMP (Koning-Delaroche, KD) and Soukhovitskii deformed optical model potential. Results are shown in Figure 9 where calculations performed with spherical and deformed optical potentials are compared with measurements. It seems that in the case of photonuclear reactions, the (γ, n), $(\gamma, 2n)$ and (γ, f) cross sections are not very sensitive to optical model parameters.

Finally, level density parameters and fission parameters were adjusted simultaneously in order to reproduce the experimental data. Adjustable level density parameters and their values are discussed in section 2.3. Final fission barrier heights, widths and transitions states are listed in section 2.4. The comparison between final calculations and measurements is given in Figure 10 up to 130 MeV.

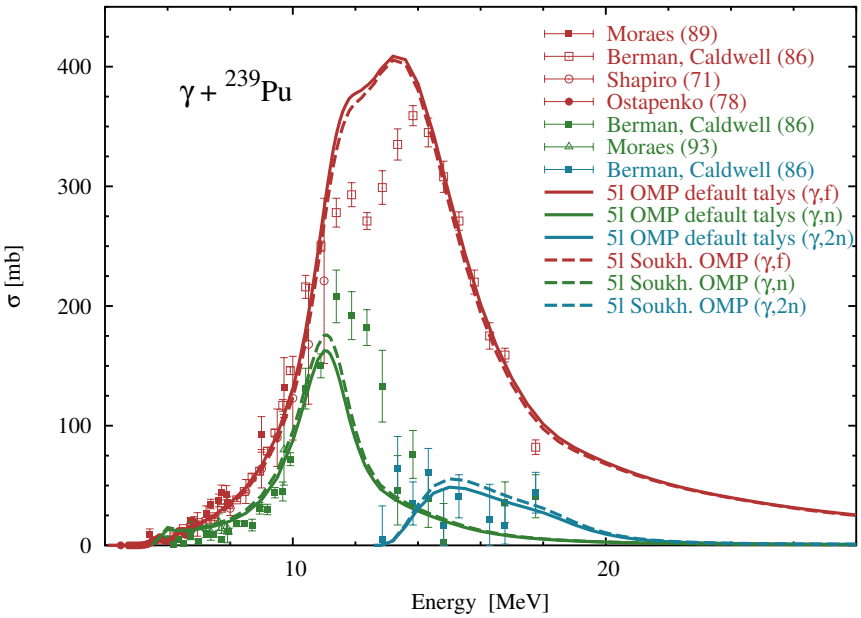

Figure 9: ^{239}Pu (γ, n), $(\gamma, 2n)$ and (γ, f) cross sections using default talys (solid line) and Soukhovitskii *et al.* [16] (dashed line) optical potential.

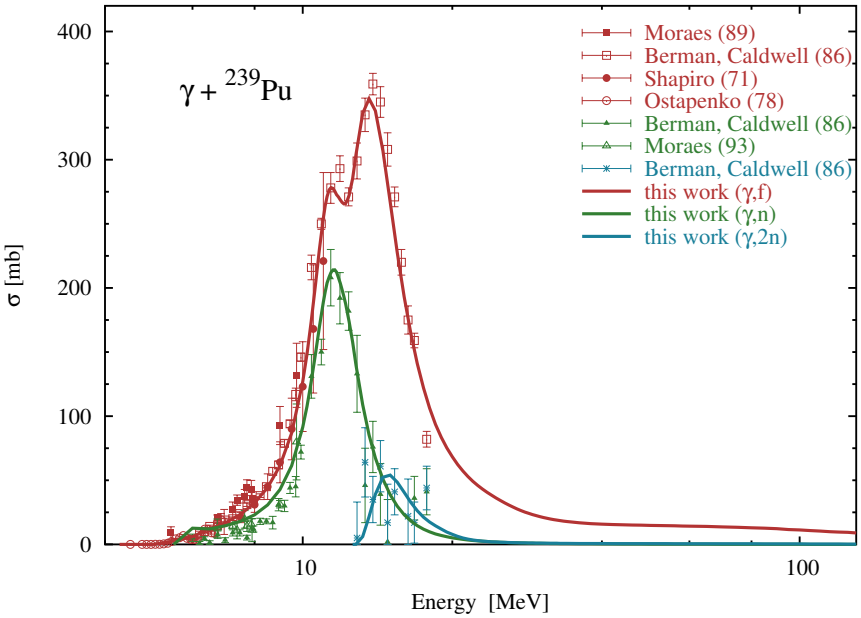

Figure 10: ^{239}Pu (γ, n), $(\gamma, 2n)$ and (γ, f) cross sections using Soukhovitskii *et al.* [16] optical potential with adjusted ^{237,238}Pu level densities and ^{237,238,239}Pu fission parameters

4 Conclusions

The photonuclear reactions on ^{239}Pu were calculated up to 130 MeV with consistent models implemented in the Talys code. A few sensitive nuclear parameters were fine-tuned to better reproduce the experimental data available for (γ, n), $(\gamma, 2n)$ and (γ, f) partial cross sections. In addition, the nuclear models provide predictions of the emitted neutron energy and angular distributions. Eventually, these results will be transformed into the standard ENDF format and recent measurements of delayed neutron yields performed at CEA [33] will complement this evaluation effort. The outcome will be proposed for insertion into the Joint Evaluated Fission and Fusion (JEFF) library to answer application needs.

References

[1] M.B. Chadwick, P. Oblozinsky, A.I. Blokhin, T. Fukahori, Y. Han, Y-O. Lee, M.N. Martins, S.F. Mughabghab, V.V. Varlamov, B. Yu, and J. Zhang. IAEA-TECDOC-1178, Vienna, http://www-nds.iaea.org/photonuclear/. 2000.

[2] M-L. Giacri-Mauborgne, D. Ridikas, M.B. Chadwick, P.G. Young, and W.B. Wilson. *Nucl. Sci. Eng.*, 153:33, 2006.

[3] P.G. Young *et al.* Los Alamos National Laboratory Report LA-12343-MS. 1992.

[4] M.B. Chadwick *et al. Nucl. Sci. Eng.*, 144:157, 2003.

[5] I. Raškinytė, E. Dupont, and D. Ridikas. *CEA Saclay Report, DAPNIA-06-101*, 2006.

[6] I. Raškinytė, E. Dupont, B. Morillon, and D. Ridikas. *Conf. on Nuclear Reaction Mechanisms, Varenna (Italy), June 12-16, 2006*, CEA Saclay Report, DAPNIA-06-147.

[7] A.J. Koning, S. Hilaire, and M.C. Duijvestijn. *Conf. on Nuclear Data for Sciece and Technology (ND2004), Santa Fe, NM (USA), September 26 - October 1, 2004.*

[8] M.B. Chadwick, P. Oblozinsky, P.E. Hodgson, and G. Reffo. *Phys. Rev. C*, 44:814, 1991.

[9] EXFOR. *http://www-nds.iaea.org/exfor/exfor00.htm.*

[10] B.L. Berman, J.T. Caldwell, E.J. Dowdy, S.S. Dietrich, P. Meyer, and R.A. Alvarez. *Phys. Rev. C*, 34:2201, 1986.

[11] M.A.P.V. De Moraes and M.F. Cesar. *Physica Scripta*, 47:519, 1993.

[12] A. Shapiro and W.F. Stubbins. *Nucl. Sci. Eng.*, 45:47, 1971.

[13] Yu. B. Ostapenko, G.N. Smirenkin, A.S. Soldatov, V.E. Zhuchko, and Yu.M. Tsipenyuk. *Yad. Konst.*, 3(30):3, 1978.

[14] G.M. Gurevich, L.E. Lazareva, V.M. Mazur, G.V. Solodukhov, and B.A. Tulupov. *Nucl. Phys. A*, 273:326, 1976.

[15] IAEA-CRP, Reference Input Parameter Library (RIPL), IAEA-TECDOC-1034, Vienna, http://www-nds.iaea.org/ripl/. 1998.

[16] E.Sh. Soukhovitskii, S. Chiba, J. Lee, O. Iwamoto, and T. Fukahori. *J. Phys. G: Nucl. Part. Phys.*, 30:905, 2004.

[17] J.A. Harvey, N.W. Hile, F.G. Perey, G.L. Tweed, L. Leal, and H. Derrien. *Conf. on Nuclear Data for Science and Technology, Mito (Japan)*, 1988.

[18] W.P. Poenitz and J.F. Whalen. *Argonne National Laboratory Reports*, 80, 1983.

[19] W.P. Poenitz, J.F. Whalen, and A.B. Smith. *Nucl. Sci. Eng.*, 78:333, 1981.

[20] T.P. Bakalov, A.A. Van'kov, Ju.V. Grigor'ev, N.B. Yaneva, G.L. Ilchev, S.A. Toshkov, V.F. Ukraintsev, and Chan khan may. *Atomnaya Energiya*, 48:377, 1980.

[21] R.B. Schwartz, R.A. Schrack, and H.T. Heaton Ii. *Nucl. Sci. Eng.*, 54:322, 1974.

[22] A.B. Smith, P. Guenther, and J. Whalen. *Journal of Nuclear Energy*, 27:317, 1973.

[23] K.A. Nadolny, F.L. Green, and P. Stoler. *Report to the U.S. Nuclear Data Comm.*, 9:170, 1973.

[24] J. Cabe and M. Cance. *CEA Saclay Reports*, 4524, 1973.

[25] D.G. Foster Jr and D.W. Glasgow. *Phys. Rev. C*, 3:576, 1971.

[26] L.F. Hansen, B.A. Pohl, C. Wong, R.C. Haight, and Ch. Lagrange. *Phys. Rev. C*, 34:2075, 1986.

[27] G. Haouat, J. Lachkar, Ch. Lagrange, Y. Patin, J. Sigaud, and R.E. Shamu. *Nucl. Sci. Eng.*, 81:491, 1982.

[28] M. Coppola and H.H. Knitter. *Zeitschrift fuer Physik*, 232:286, 1970.

[29] R. Batchelor and K. Wyld. *A.W.R.E. Aldermaston Reports*, 55, 1969.

[30] A. Gilbert and A.G.W. Cameron. *Can. J. Phys.*, 43:1446, 1965.

[31] P. Demetriou and S. Goriely. *Nucl. Phys. A*, 695:95, 2001.

[32] A.V. Ignatyuk, G.N. Smirenkin, and A.S. Tishin. *Sov. J. Nucl. Phys.*, 21:255, 1975.

[33] A. Vanlauwe *et al. Conf. on Nuclear Reaction Mechanisms, Varenna (Italy), June 12-16, 2006*, CEA Saclay Report, DAPNIA-06-161.